

---

# Causal Generative Domain Adaptation Networks

---

Mingming Gong <sup>\*1,2</sup> Kun Zhang <sup>\*2</sup> Biwei Huang <sup>2</sup> Clark Glymour <sup>2</sup> Dacheng Tao <sup>3</sup> Kayhan Batmanghelich <sup>1</sup>

## Abstract

We propose a new generative model for domain adaptation, in which training data (source domain) and test data (target domain) come from different distributions. An essential problem in domain adaptation is to understand how the distribution shifts across domains. For this purpose, we propose a generative domain adaptation network to understand and identify the domain changes, which enables the generation of new domains. In addition, focusing on single domain adaptation, we demonstrate how our model recovers the joint distribution on the target domain from unlabeled target domain data by transferring valuable information between domains. Finally, to improve transfer efficiency, we build a causal generative domain adaptation network by decomposing the joint distribution of features and labels into a series of causal modules according to a causal model. Due to the modularity property of a causal model, we can improve the identification of distribution changes by modeling each causal modules separately. With the proposed adaptation networks, the predictive model on the target domain can be easily trained on data sampled from the learned networks. We demonstrate the efficacy of our method on both synthetic and real data experiments.

## 1. Introduction

In recent years supervised learning has achieved great success in various real-world applications, such as visual recognition, speech recognition, and natural language processing. However, supervised learning methods, especially deep learning techniques, typically require a large amount of labeled data, which is difficult and expensive to obtain for many applications. Also, even when access to large-scale

training data is possible, the resulting predictive model may not generalize well when the distribution of the test domain is significantly different. For example, a predictive model trained with data from one hospital may fail to produce reliable prediction in a different hospital due to distribution change. Domain adaption (DA) aims at learning models that can generalize well to new domains by transferring useful information across source and target domains. In this paper we focus on unsupervised DA, where no labeled data are provided on the target domain.

A critical problem in domain adaption is to understand how the distribution changes across domains. Let  $X$  denote the features and  $Y$  the labels. A large body of previous methods assume that the marginal distribution  $P_X$  changes but  $P_{Y|X}$  stays the same, i.e., the *covariate shift* situation (Shimodaira, 2000; Huang et al., 2007; Bakdashmotlagh et al., 2013). In this situation, correcting the shift in  $P_X$  is a relative easy task because it does not require any labeled data. In this paper, we focus on the more general *conditional shift* (Zhang et al., 2013) situation where  $P_{X|Y}$  changes, leading to simultaneous changes in  $P_X$  and  $P_{Y|X}$ . In this case, understanding how  $P_{X|Y}$  changes is essential to identify the target domain  $P_{X|Y}$  from unlabeled target domain data. (Zhang et al., 2013; Gong et al., 2016) assumed simple location-scale transforms of  $P_{X|Y}$  and found the identifiability conditions. However, the location-scale transform is easily violated in practical applications, calling for more general modeling of distribution changes.

In this paper, we propose a generative domain adaptation network (GDAN) to understand how  $P_{X|Y}$  changes across domains and generate new domains. The proposed network models the function  $X = g(Y, E, \theta)$  which generates  $X$  conditioned on  $Y$  and domain-specific parameter  $\theta$ . When  $\theta$  changes, we can obtain different domains with different conditional distributions  $P_{X|Y, \theta}$ . Assuming  $\theta$  is low-dimensional, we provide the necessary conditions for the identifiability of distribution changes from multiple source domains. Furthermore, we focus on the more challenging single source domain adaptation problem in which we only have two domains and one of them is unlabeled. We show under mild conditions that  $\theta$  is also identifiable in single domain adaptation. Inspired by generative adversarial networks (GAN) (Goodfellow et al., 2014), we estimate the parameters of the neural networks and the domain parameter

<sup>\*</sup>Equal contribution <sup>1</sup>Department of Biomedical Bioinformatics, Pittsburgh, PA, USA <sup>2</sup>Department of Philosophy, Carnegie Mellon University, Pittsburgh, PA, USA <sup>3</sup>UBTECH Sydney AI Centre, SIT, FEIT, The University of Sydney, Australia. Correspondence to: Mingming Gong <gongmingju@gmail.com>.

$\theta$  by adversarial training. Our model enables us to generate a new domain by interpolation in the  $\theta$  space. It also allows us to train more accurate predictive models for the target domain by making use of generated data.

To further improve transfer efficiency, we propose to factorize the joint distribution of features and labels according to a causal model that is assumed to be fixed across domains. Then we build a causal generative domain adaptation network (C-GDAN) following the causal structure. Benefiting from the modularity/invariance property of a causal model, we can decompose  $\theta$  into unrelated, separate sets of parameters, each of which corresponds to a causal module/factor. Then it is easier to interpret the parameters and find valid regions of the parameters corresponding to reasonable data. In addition, in the presence of multiple source domains, we are able to identify the changing causal modules and thus reduce the dimension of  $\theta$ .

## 2. Related Work

Domain adaptation has been extensively studied in the past decade, and here we focus on most related unsupervised DA methods. In the covariate shift scenario, to correct the shift in  $P_X$ , earlier approaches reweight the source domain data by density ratios estimated from unlabeled data in both domains (Shimodaira, 2000; Sugiyama et al., 2008; Huang et al., 2007). The reweighted source domain data provide an unbiased estimate of the target domain marginal distribution (Cortes et al., 2010; Yu & Szepesvári, 2012). However, this type of methods require the target domain to be contained in the support of the source domain, which can be violated in many applications. Another line of methods search for a domain-invariant representation that has similar distributions on both domains. These methods rely on various distance discrepancy measures as the objective functions to match representation distributions, including maximum mean discrepancy (MMD) (Pan et al., 2011; Baktashmotlagh et al., 2013), separability measured by discriminative classifiers (Ganin et al., 2016), and optimal support (Courty et al., 2017b;a). Also, the representation learning architecture have developed from shallow architectures such as linear projections (Pan et al., 2011; Baktashmotlagh et al., 2013) to deep neural networks (Tzeng et al., 2014; Long et al., 2015; Ganin et al., 2016).

Recently, another line of works attempt to address the more challenging situation where  $P_X$  and  $P_{Y|X}$  change simultaneously across domains. This kind of methods typically assumes a causal generative model  $Y \rightarrow X$ , factorize joint distribution following the causal direction as  $P_{XY} = P_Y P_{X|Y}$ , and consider the changes in  $P_Y$  and  $P_{X|Y}$  independently. (Storkey, 2009; Zhang et al., 2013; Iyer et al., 2014) assumed only changes in  $P_Y$  and proposed principled methods to estimate  $P_Y$  in the target domain by matching marginal

distributions. The identifiability of target domain  $P_Y$  is theoretically guaranteed under mild conditions. (Zhang et al., 2013; Gong et al., 2016) further considered the changes in  $P_{X|Y}$ , known as *generalized target shift* and proposed representation learning methods with identifiability justifications, i.e., the learned representation  $\tau(X)$  has invariant  $P_{\tau(X)|Y}$  across domains if  $P_{\tau(X)}$  is invariant after correction for  $P_Y$ . This also explains why previous representation learning methods for correcting covariate shift can work in the *conditional shift* situation where only  $P_{X|Y}$  change but  $P_Y$  remains the same. Following this line, (Courty et al., 2017a) proposed a joint optimal transport method which match joint distributions iteratively using estimated target domain labels. (Long et al., 2017) proposed a deep joint adaptation method matching the joint distribution of multi-layer features in a convolutional neural network (CNN).

Unsupervised image translation, which aims to transform images in one domain to another one without correspondences, is a closely related problem to unsupervised DA. If the images can be successfully translated from the source domain to the target domain, we can use the translated images and the corresponding source domain labels to train a learning machine for the target domain (Bousmalis et al., 2017). Unsupervised image translation is usually achieved by learning a generative adversarial network that maps source domain images to a fake domain on which the distribution matches the distribution on the target domain (Liu et al., 2017; Li et al., 2017b; Kim et al., 2017). To improve identifiability, some constrained networks have been proposed, such as the cycle-consistency GAN (Zhu et al., 2017) and the coupled GAN (Liu & Tuzel, 2016). Though image translation can be a possible solution to domain adaptation, it is actually a much harder problem because it requires identifiability in the image level, while domain adaption only requires identifiability w.r.t. the class labels.

## 3. Preliminary

### 3.1. Maximum Mean Discrepancy

The kernel mean embedding of distributions is an important mathematical tool to represent and compare distributions (Huang et al., 2007; Muandet et al., 2017). Let  $\mathcal{H}$  denote a characteristic reproducing kernel Hilbert space (RKHS) on the input feature space  $\mathcal{X}$  associated with a kernel  $k(\cdot, \cdot) : \mathcal{X} \times \mathcal{X} \rightarrow \mathbb{R}$ , and  $\phi$  be an associated mapping such that  $\phi(x) \in \mathcal{H}_x$ . Similarly, we define a RKHS  $\mathcal{H}_y$  on the label space  $\mathcal{Y}$  associated with kernel  $l(\cdot, \cdot) : \mathcal{Y} \times \mathcal{Y} \rightarrow \mathbb{R}$  and mapping  $\psi$ . The kernel embedding of a distribution  $P_X$  can be formulated as  $\mu_{P_X} = E_{X \sim P_X}[\phi(X)]$ , which can be easily extended to embed a joint distribution  $P_{XY}$  as  $\mu_{P_{XY}} = E_{(X,Y) \sim P_{XY}}[\phi(X) \otimes \psi(Y)]$ , where  $\otimes$  denotes tensor product (Song et al., 2013). Given two probability distributions  $P_X$  and  $Q_X$ , we can use squared MMD to mea-

sure the distance between them:  $M_k = \|\mu_{P_X} - \mu_{Q_X}\|_{\mathcal{H}_x}^2$ . It can be extended to compare joint distributions  $P_{XY}$  and  $Q_{XY}$  by  $J_{kl} = \|\mu_{P_{XY}} - \mu_{Q_{XY}}\|_{\mathcal{H}_x \otimes \mathcal{H}_y}^2$ .

### 3.2. Generative Adversarial Networks

Given a sample  $\{x_i\}_{i=1}^n$  drawn from  $P_X$ , GAN trains a generator  $g$  to transform noises  $E$  sampled from a canonical distribution  $P_E$  into  $g(E)$  such that  $P_{g(E)} \approx P_X$ . The distance between  $P_X$  and  $P_{g(E)}$  is measured by their samples  $\{x_i\}_i^n$  and  $\{e_i\}_i^n$ . The original GAN uses the separability of a discriminative classifier  $f$  as a distance measure and play a two-player game to find  $g$  and  $f$  iteratively. Generative moment matching network (GMMN) (Li et al., 2015) adopts MMD as the distribution discrepancy measure and learn the generator by

$$\min_g M_k(P_X, P_{g(E)}). \quad (1)$$

Because GMMN does not work well on complex distributions, (Li et al., 2017a) proposed to learn the kernel simultaneously by function composition, resulting in the kernel  $\tilde{k} = k \circ f$ , where  $\tilde{k}(x, x') = k(f(x), f(x'))$ . The parameters in the generator and the composition function are learned by

$$\min_g \max_f M_{k \circ f}(P_X, P_{g(E)}), \quad (2)$$

In image generation,  $f$  can be chosen as convolutional neural networks to generate more realistic images. In this paper, we also rely on MMD as the distribution discrepancy measure because it is easily extensible to matching joint distributions.

## 4. Generative Domain Adaptation Network

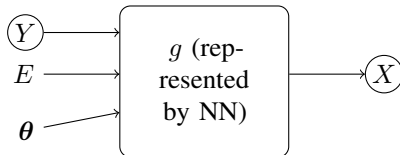


Figure 1. Generative domain adaptation network.

In unsupervised DA, we are given  $m$  source domains  $\mathcal{D}_s = \{(x_i^s, y_i^s)\}_{i=1}^{n_s} \sim P_{XY}^s$ , where  $s \in \{1, \dots, m\}$  and a target domain  $\mathcal{D}_t = \{x_i^t\}_{i=1}^{n_t}$  of  $n_t$  labeled examples sampled from  $P_X^t$ . In this paper we try to answer the following two questions. First, is it possible to identify the changing parameters in  $P_{X|Y}$  from multiple source domains? If the changing parameters can be identified, we can understand the domain changes and generate new domains. Second, in the extreme case when only one source domain is available, can we recover the joint distribution  $P_{XY}^t = P_{X|Y}^t P_Y^t$  and train a predictive model for the target domain?

To answer the above two questions, we propose the generative domain adaptation network (GDAN) to model distribution changes across domains. As shown in Figure 1, we consider the data generating model

$$X = g(Y, E, \theta), \quad (3)$$

which transforms random noise  $E \sim P_E$  to  $X \in \mathbb{R}^D \sim Q_{X|Y}$  conditioned on  $Y$  in a domain associated with parameter  $\theta \in \mathbb{R}^d$ . The generator approximates the class conditional distribution  $P_{X|Y}$  in each domain.  $E$  is independent of  $Y$  and has a fixed distribution across domains.  $g$  is a generator represented by a neural network (NN) and is shared by all domains.  $\theta$  has different values on different domains and thus encodes the changes of  $P_{X|Y}$  across domains. One can also consider  $\theta$  as a latent variable, whose value on the  $s$ -th domain is denoted as  $\theta_s$ .

### 4.1. Identifiability

Suppose the data were generated from model (3). It is essential see to whether  $\theta$  is identifiable from data. Here identifiability means there is a one-to-one mapping between the estimated parameters  $\hat{\theta}$  and true parameters, which further indicates that the estimated  $\hat{\theta}$  can capture all the distribution changes.

If  $\theta$  is high-dimensional, intuitively, it means that the changes in  $P_{X|Y}$  are complex; in the extreme case, it could change arbitrarily across domains. In this case, one might not be able identify  $g$  and  $\theta$  if having only a small number of source domains. In contrast, if  $\theta$  is low-dimensional, identification of  $\theta$  will become much easier. In the following, we will present the identifiability results of our model in the linear case. We make the following assumptions on the model.

A1. The generator  $g$  is linear. (3) can be represented as

$$X = A_1 E + A_2 Y + A_3 \theta. \quad (4)$$

A2. The columns of  $A_3$  are linearly independent.

A3. The dimension of  $X$  is greater than that of  $\theta$ , i.e.,  $D \geq d$ .

A4.  $\theta$  is Gaussianly distributed across domains, i.e.,  $\theta_s$  on the  $s$ -th domain is sampled from  $\mathcal{N}(0, I_d)$ , where  $I_d$  is a  $d \times d$  identity matrix.

**Theorem 1.** Suppose the  $s$ -th source domain data were generated from the model (4) with  $\{A_i\}_{i=1}^3$  and  $\theta_s$ . Denote  $\Theta \in \mathbb{R}^{d \times m}$  as a matrix whose  $s$ -th column is  $\theta_s$ , if  $\text{rank}(\Theta) \geq d+1$  (a necessary condition is  $m \geq d+1$ ) and A1-A4 hold true, by matching the joint distributions  $P_{XY}^s$  on the source domains and the distributions  $Q_{XY}^s$  obtained

by model (4) with  $\{\hat{A}_i\}_{i=1}^3$  and  $\hat{\theta}_s$ , then  $\hat{\theta}$  is a one-to-one mapping of  $\theta$  (i.e.,  $\hat{\theta} = h(\theta)$ ), where  $h$  is an invertible function.

A complete proof of Theorem 1 can be found in Section S1 of Supplementary Material. From Theorem 1, we can see that if the number of domains is smaller than the dimension of  $\theta$ , matrix  $\hat{A}_3^\top A_3$  will be rank deficient, and there is no one-to-one mapping between  $\hat{\theta}$  and  $\theta$ , which means the distribution changes cannot be fully captured by the estimated parameters of the proposed model. Though our proof assumes a linear system<sup>1</sup>, it shows the necessity of multi-source domains when the distribution changes are large. In practice, if the  $\theta$  values do not vary largely across domains, we can assume that  $g$  is approximately linear w.r.t.  $\theta$ . That is to say, if  $g$  is nonlinear, we need at least  $d + 1$  domains in a local region bounded by the  $\theta$  values.

In practice, we often encounter the most challenging situation when there is only one source domain. In this case, we must incorporate the target domain to learn the distribution changes. According to Theorem 1, one dimensional change can be fully identified in the linear case if target domain has labels. However, due to the absence of labels on the target domain, the identifiability of  $\theta$  needs more assumptions, which are stated as follows.

A5. Assume  $Y \in \{1, \dots, C\}$ . Denote  $P_{X|Y,\theta}$  the conditional distribution of  $X$  generated by  $X = g(Y, E, \theta)$ . For any  $\theta$  and  $\theta'$ , the elements in the set  $\{\lambda P_{X|Y=c,\theta} + \lambda' P_{X|Y=c,\theta'}; c = 1, \dots, C\}$  are linearly independent  $\forall \lambda, \lambda' (\lambda^2 + \lambda'^2 \neq 0)$ .

**Theorem 2.** Suppose A5 holds true. Given two models in the form of (3) with parameters  $\theta$  and  $\theta'$ . Given two class prior  $P_Y$  and  $P'_Y$ , if the marginal distributions of the generated  $X$  satisfy  $P_{X|\theta} = P_{X|\theta'}$ , then  $P_{X|Y,\theta} = P_{X|Y,\theta'}$  and  $P_Y = P'_Y$ .

A complete proof of Theorem 2 can be found in Section S2 of Supplementary Material. If we can learn the shared generator  $g$  from source domains, given a new unlabeled domain, we only need to estimate  $\theta$  to obtain the generative model for the new domain. Because the dimensionality of  $\theta$  is low, each conditional distribution  $P_{X|Y=c}$  tends to change in its own manifold, which makes it easier for A5 to hold true. In single-source domain adaptation, we have to estimate  $g$  and  $\theta$  simultaneously from two domains one of which is unlabeled. In this case, even if A5 is true, learning is more difficult because estimations of  $g$  and  $\theta$  are coupled with each other.

<sup>1</sup>we note that identifiability for nonlinear systems is important. To give this proof is nontrivial and is a line of our future work.

## 4.2. Adversarial Training

**Reparameterization** In the proposed GDAN, since the input to the neural network involves an unknown domain parameter  $\theta$ , we cannot directly use adversarial training strategies to estimate our model parameters. To enable adversarial training, we reparameterize  $\theta$  by a linear transformation of the one-hot representation  $1_s$  of domain index  $s$ , i.e.,  $\theta = \Theta 1_s$ . Consequently, we can reparameterize the generator  $g$  to  $g'(Y, E, S)$  where  $\Theta$  is absorbed into  $g'$ ,  $S$  is random variable representing domain index.

The reparameterized generator is a conditional GAN generator conditioned on  $Y$  and  $S$ . However, this is different from the usual conditional GAN generator  $g(Y, E, S)$  which directly takes the one-hot representations of  $Y$  and  $S$  as inputs. The first reason why we separate  $\theta$  out is because the domain index does not contain rich domain specific information. If we want to generate new domains, we can do interpolation in the  $\theta$  space instead of the one-hot representation space. Second, by setting the dimensionality of  $\theta$  to  $L$ , our generator reduces to the common conditional GAN generator. That is to say, our generator has a way to control the dimensionality of  $\theta$  while the common conditional GAN generator does not.

**Objective function** On the  $s$ -th source domain, we estimate the the model by matching the joint distributions  $P_{XY}^s$  and  $Q_{XY}^s$ , where  $Q_{XY}^s$  is the joint distribution of the generated features  $X = g'(Y, E, S = s)$  and labels  $Y$ . Specifically, the generator  $g$  and the discriminator  $f$  is learned by

$$\min_{g'} \max_f J_{(k \circ f)l} = \|\mu_{P_{XY}^s} - \mu_{Q_{XY}^s}\|_{\mathcal{H}_x \otimes \mathcal{H}_y}^2. \quad (5)$$

In practice, given a mini-batch of size  $n$  consisting of  $\{(x_i^s, y_i^s)\}_{i=1}^n$  sampled from the source domain data and  $\{(\hat{x}_i^s, \hat{y}_i^s)\}_{i=1}^n$  sampled from the generator, we learn the parameters by employing the empirical joint MMD, which is defined as

$$\begin{aligned} \hat{J}_{(k \circ f)l}^s &= \frac{1}{n^2} \sum_i^n \sum_j^n k(f(x_i^s), f(x_j^s))l(y_i^s, y_j^s) \\ &\quad - \frac{2}{n^2} \sum_i^n \sum_j^n k(f(x_i^s), f(\hat{x}_j^s))l(y_i^s, \hat{y}_j^s) \\ &\quad + \frac{1}{n^2} \sum_i^n \sum_j^n k(f(\hat{x}_i^s), f(\hat{x}_j^s))l(\hat{y}_i^s, \hat{y}_j^s) \end{aligned} \quad (6)$$

On the target domain, since we do not have groundtruth labels, we propose to match the marginal distributions  $P_X^t$  and  $Q_X^t$ , where  $Q_X^t$  is the marginal distribution of generated features  $X = g'(Y, E, S = m + 1)$ . Given a mini-batch of size  $n$  consisting of  $\{x_i^t\}_{i=1}^n$  sampled from the target

domain data and  $\{\hat{x}_i^t\}_{i=1}^n$  sampled from the generator, the loss function on the target domain is the empirical MMD:

$$\begin{aligned}\hat{M}_{(k \circ f)} &= \frac{1}{n^2} \sum_i^n \sum_j^n k(f(x_i^t), f(x_j^t)) \\ &\quad - \frac{2}{n^2} \sum_i^n \sum_j^n k(f(x_i^t), f(\hat{x}_j^t)) \\ &\quad + \frac{1}{n^2} \sum_i^n \sum_j^n k(f(\hat{x}_i^t), f(\hat{x}_j^t)).\end{aligned}\quad (7)$$

Finally, we learn the mode parameter on the source and target domains simultaneously by combining the source and target domain objectives:

$$\min_{g'} \max_f L = \frac{1}{m} \sum_{s=1}^m \hat{J}_{(k \circ f)l}^s + \lambda \hat{M}_{(k \circ f)}, \quad (8)$$

where  $\lambda$  is hyperparameter that balances the loss on source and target domains.

## 5. Causal Generative Domain Adaptation Networks

Although multi-layer perceptron (MLP) is a good function estimator, it is highly overparameterized. Thus, reducing the model complexity by incorporating structures into the network is critical for efficient learning. For example, the fractional convolutional networks have significantly outperformed MLPs on natural image generation. However, there are many kinds of data which cannot benefit from convolutional structures. In this section, we present our causal generative domain adaptation network (C-GDAN) which is built on the causal structure between the features that are relevant to the labels.

### 5.1. Causal Factorization

We will model the distribution of  $Y$  and relevant features following a graphical representation. From a causal perspective, we factorize and model the distribution according to the causal model, which is assumed to be the same on all domains. Roughly speaking, the causal process usually admits a simpler representation than the model in the anti-causal direction. (In some cases, such as the one with linear causal relations between variables with Gaussian distributions, the models may be equally simple or complex.) Therefore we prefer to learn how the distribution changes according to the causal factorization. However, note that in this paper our goal is not to do causal discovery, but to make prediction by making use of properties of the changes in the data distribution. We employ *causal Bayesian networks* to represent the causal relations between variables. The definition is as follows (Spirtes et al., 2001; Pearl, 2000).

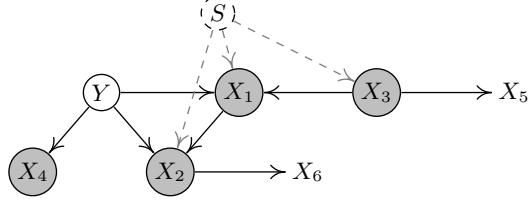


Figure 2. A graphical model over  $Y$  and features  $X_i$ .  $Y$  is the variable to be predicted, and nodes in gray are in its Markov Blanket.  $S$  denotes the domain index; a direct link from  $S$  to a variable indicates that the generating process for that variable changes across domains. Here the generating processes for  $Y$ ,  $X_1$ ,  $X_2$ , and  $X_3$  vary across domains.

**Definition 1.** Let  $\mathcal{G} = (\mathbf{V}, \mathcal{E})$  be a DAG over a set of variables  $\mathbf{V} = \{X_1, \dots, X_D\}$ , and  $P$  be a joint distribution over  $\mathbf{V}$ . The pair  $\langle \mathcal{G}, P \rangle$  is a causal Bayesian network ( $\mathcal{G}$  is called a causal DAG or a Pearlian DAG), if the following assumptions hold.

1. **Representational assumptions** The exists some directed acyclic graph (DAG)  $\mathcal{G}$  that can represent the causal structure of a system.
2. **Causal Markov condition** The  $d$ -separations in  $\mathcal{G}$  are embodied as conditional independencies in the distribution  $P(\mathbf{V})$ . If the causal Markov condition is satisfied, the distribution  $P$  admits a causal factorization  $P(\mathbf{V}) = \prod_{i=1}^D P(X_i | \mathbf{PA}_i^{\mathcal{G}})$ .
3. **Modularity/Invariance** For any variable  $X_i \in \mathbf{V}$ , the causal process producing its value from its parents, defined by conditional distribution  $P(X_i | \mathbf{PA}_i^{\mathcal{G}})$ , is unaltered no matter which variables in the system (other than  $X_i$  itself) are intervened on.

In this paper, we assume the labels  $Y$  and domain index  $S$  to be the root causes for the features  $X_i$  and reply on causal discovery algorithms to discover the causal relations among  $X_i$ . Figure 2 shows a DAG over  $Y$ ,  $S$ , and features  $X_i$ . According to the causal Markov condition, the distribution over  $Y$  and the variables in its Markov Blanket (gray nodes) can be factorized according to the DAG as

$$P_{XY} = P_Y P_{X_1|Y, X_3} P_{X_2|X_1, Y} P_{X_3} P_{X_4|Y}. \quad (9)$$

We only consider the Markov blanket  $MB(Y)$  of  $Y$  because of the following conditional independence property:

$$P_{Y|X} = P_{Y|MB(Y), MB(Y) \setminus X} = P_{Y|MB(Y)}. \quad (10)$$

Making use of this conditional independence property, we can reduce the parameters in our generative model without hurting the prediction performance.

Based on the causal Markov condition, we can factorize the joint distribution and model the conditional distribution of each factor separately. Furthermore, under the modularity/invariance assumption, we can also model the changes in each factor separately. For example, if  $S$  is only connected to  $X_1$ , then only the factor  $P_{X_1|Y, X_3}$  is subject to changes across domains. In addition, as will be shown in Sec 5.3, we can apply a recent causal discovery method to detect the changing modules and further reduce the number of changing parameters. In Figure 2, the joint distributions over  $Y$  and  $MB(Y)$  on the source and target domain can be represented as

$$\begin{aligned} P_{XY}^s &= P_Y P_{X_1|Y, X_3}^s P_{X_2|X_1, Y}^s P_{X_3}^s P_{X_4|Y}^s \text{ and} \\ P_{XY}^t &= P_Y P_{X_1|Y, X_3}^t P_{X_2|X_1, Y}^t P_{X_3}^t P_{X_4|Y}^t, \end{aligned} \quad (11)$$

respectively, where the two factors  $P_Y$  and  $P_{X_4|Y}$  are constant across domains. In the following section, we will show how to represent the distribution and distribution changes by functional causal models, which can be implemented using neural networks.

## 5.2. Network Construction

We will construct a causal generative domain adaptation network by using neural networks to implement a functional causal model (FCM) (Pearl, 2000). In a FCM, causal relationships are described by deterministic *functional* equations, each of which explains one variable in the causal system in terms of its direct causes. Probabilities are introduced through the unobserved random noise variables which are often assumed to be independent from each other.

In its general form, a FCM is a tuple  $\langle \mathbf{S}, P \rangle$  which consists of a set of equations  $\mathbf{S} = (S_1, \dots, S_D)$ :

$$S_i : X_i \leftarrow F_i(\mathbf{PA}_i, E_i), \quad i = 1, \dots, D, \quad (12)$$

and a probability distribution  $P$  over  $\mathbf{E} = (E_1, \dots, E_D)$ .  $\mathbf{PA}_i$  denotes the direct causes of  $X_i$ , and  $E_i$  represents noises or errors due to unobserved factors.  $E_i$  are required to be jointly independent. In this paper, we assume that all the noise  $\{E_i\}_{i=1}^n$  follow Gaussian distributions.

The causal factorizations according to a causal DAG can be represented by a FCM. For example, Eq. (9) can be represented by the following FCM:

$$\begin{aligned} Y &\leftarrow E_0, \quad X_3 \leftarrow F_3(E_3), \quad X_1 \leftarrow F_1(Y, X_3, E_1), \\ X_2 &\leftarrow F_2(Y, X_1, E_2), \quad X_4 \leftarrow F_4(Y, E_4), \end{aligned} \quad (13)$$

where  $E_0$  has the same distribution as  $Y$  and the distribution can be estimated from source domain labels.  $E_1, \dots, E_4$  are assumed to be Gaussianly distributed. When the distribution changes across domains, we assume that only the functions  $F_i$  change, but the noise distributions are fixed.

To model the changes more compactly in the FCM, we extend the FCM by incorporating the domain variables  $\{\theta_1, \dots, \theta_D\}$ , i.e,

$$S_i : X_i \leftarrow g_i(\mathbf{PA}_i, E_i, \theta_i), \quad i = 1, \dots, D, \quad (14)$$

where  $g_i$  is a fixed function for both domains and the changes are modeled by  $\theta_i$ . It is worth noting that, due to the modularity assumption, changes in  $\theta_i$  values only affects the conditional distribution  $P_{X_i|\mathbf{PA}_i}$ .

Based on (14), we employ a neural network to model each  $g_i$  separately, and construct a constrained generative model according to the causal DAG, which we call a causal generative domain adaptation network (C-GDAN). By using the reparameterization trick in section 4.2 for each  $\theta_i$ , we can learn the network parameters using the adversarial training procedure described in Section 4.2. Figure 3 illustrates part of the network constructed according to the DAG in Figure 2 over  $Y$ ,  $X_1$ , and  $X_2$ .

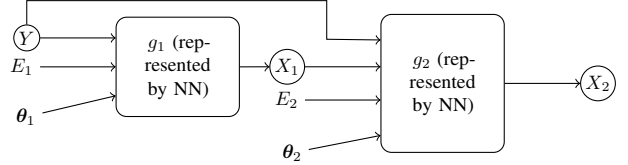


Figure 3. The causal generative domain adaptation network for with modules  $Y \rightarrow X_1$  and  $(Y, X_1) \rightarrow X_2$ .

**Remark** Let us make the advantages of using causal representation clear. On the one hand, by decomposing the latent variables or parameters into unrelated, separate sets of parameters  $\theta_i$ , each of which corresponds to a causal module (Pearl, 2000), it is easier to interpret the parameters and find valid regions of the parameters corresponding to reasonable data. On the other hand, even if we just use the parameter values learned from observed data, we can easily come up with new data by making use of their combinations. For instance, suppose we have  $(\theta_1, \theta_2)$  and  $(\theta'_1, \theta'_2)$  learned from two domains. Then  $(\theta_1, \theta'_2)$  and  $(\theta'_1, \theta_2)$  also correspond to valid causal processes because of the modularity property of the causal process.

## 5.3. Causal Discovery

We utilize a widely-used causal discovery approach, PC (Spirtes et al., 2001), to learn the causal graph up to the Markov equivalence class. The original PC assumes that the data are i.i.d., and the underlying causal structure is fixed on the whole data set. We add the constraint that  $Y$  is a root cause for  $X_i$  to identify the causal structure on a single source domain.

If there are multi-source domains, we modify the CD-NOD method (Zhang et al., 2017), which extends the original PC

to the case when there are distribution shifts, by adding the constraint that  $Y$  is a root cause. Also, the domain index  $S$  is added as an additional variable into the causal system to capture the heterogeneity of the underlying causal model, and we use kernel-based conditional-independence test to test the (conditional) independence (Zhang et al., 2011). CD-NOD allows us to recover the underlying causal graph robustly and detect changing causal modules. By doing so, we only need to learn  $\theta_i$  for the changing modules, which improves transfer efficiency.

Since the causal discovery methods are not guaranteed to find all the edge directions, we propose a simple solution to build a network on top a partially directed acyclic (PDAG). By removing the directed edges from the graph, we detect connected components each of which contains a group of nodes connected by undirected edges. We consider each connected component as a multivariate variable and obtain a DAG on which we can apply the network construction procedure described in Sec. 5.2.

## 6. Experiments

We now evaluate the proposed methods on both synthetic and real datasets. After introducing the implementation details, we evaluate our methods on the rotated MNIST dataset, WiFi localization dataset, and MNIST-USPS dataset. We provide both qualitative and quantitative evaluations. We incorporate structures into the network to reduce model complexity. Specifically, we employ a causal network based on the learned causal structures for WiFi localization data. Because causal relations are not believed to exist between pixels, we use the commonly used convolutional neural network for image data.

**Implementation Details** We implement all the models using PyTorch and train the models with the RMSProp optimizer (Tieleman & Hinton, 2012). We use a batch size of 64 for all image datasets and 128 for the WiFi localization dataset. We adopt the DCGAN network architecture (Radford et al., 2015), which consists of a fractional convolutional neural network for the generator  $g$  and a convolutional neural network for the discriminator  $f$ , for image datasets. For the WiFi dataset, we employ MLPs for  $g$  and use no  $f$  because MMD is complicated enough for measuring distribution discrepancy on this dataset. When  $f$  is incorporated, we use a linear kernel in MMD; otherwise, we employ a mixture of RBF kernels  $k(x, x') = \sum_{q=1}^K k_{\sigma_q}(x, x')$  in MMD. In the experiments, we fix  $K = 5$  and  $\sigma_q$  to be  $\{0.25, 0.5, 1, 2, 4\}$  times the median of the pairwise distances between all source examples.

### 6.1. Simulations: Rotated MNIST

We first conduct simulation studies on the MNIST dataset to demonstrate how distribution changes can be identified from multiple source domains. MNIST is a handwritten digit dataset including ten classes 0–9 with 60,000 training images and 10,000 test images. We rotate the images by different angles and construct domains containing rotated images. We denote a domain with images rotated by angle  $\gamma$  as  $\mathcal{D}_\gamma$ . The dimensionality of  $\theta$  is 1.

Since  $g$  is nonlinear w.r.t.  $\theta$ , one cannot expect full identification of  $\theta$  from only two domains. However, as discussed in Sec 4.1, we might be able to identify  $\theta$  within a local region from two domains if  $g$  is approximately linear w.r.t.  $\theta$  in that local region. To verify this, we conduct experiments on two synthetic datasets. One dataset contains two source domains  $\mathcal{D}_{0^\circ}$  and  $\mathcal{D}_{45^\circ}$  and the other has two source domains  $\mathcal{D}_{0^\circ}$  and  $\mathcal{D}_{90^\circ}$ . We train our model on these two datasets and obtain  $\hat{g}$  and  $\hat{\theta}$  on each domain.

To investigate whether the model is able to learn meaningful rotational changes, we sample  $\theta$  values uniformly from  $[\hat{\theta}_s, \hat{\theta}_t]$  to generate new domains.  $\theta_s$  and  $\theta_t$  are the learned domain parameter in the source and target domain, respectively. As shown in Figure 6, on the dataset with source domains  $\mathcal{D}_{0^\circ}$  and  $\mathcal{D}_{45^\circ}$ , our model successfully generates a new domain in between. This indicates that  $\theta$  in our model captures meaningful distribution changes. However, on the dataset with source domains  $\mathcal{D}_{0^\circ}$  and  $\mathcal{D}_{90^\circ}$ , although our model well fits the two source domains, the generated new domain does not correspond to the domain with rotated images, indicating that the distance between two source domains are two far away for our model to identify meaningful distribution changes.

### 6.2. Cross-Domain Indoor WiFi Localization

We then perform evaluations on the cross-domain indoor WiFi location dataset (Zhang Kai et al., 2013). The WiFi data were collected from a building hallway area, which was discretized into a space of 119 grids. At each grid point, the strength of WiFi signals received from  $D$  access points were collected by a device. We aim to predict the location of the device from the  $D$ -dimensional WiFi signals, which is casted a regression problem. The dataset contains two domain adaptation tasks: 1) transfer across time periods and 2) transfer across devices. In the first task, the WiFi data were collected by the same device during three different time periods  $t_1, t_2$ , and  $t_3$  in the same hallway. Three subtasks including  $t_1 \rightarrow t_2$ ,  $t_1 \rightarrow t_3$ , and  $t_2 \rightarrow t_3$  are taken for performance evaluation. In the second task, the WiFi data were collected by different devices, causing a distribution shift of the received signals. We evaluate the methods on three datasets, i.e., `hallway1`, `hallway2`, `hallway3`, each of which contains data collected by two different devices in

Table 1. Comparison of different methods on the WiFi dataset.

	KRR	TCA	SuK	DIP	CTC	GDAN	C-GDAN
$t_1 \rightarrow t_2$	$80.84 \pm 1.14$	$86.85 \pm 1.1$	<b><math>90.36 \pm 1.22</math></b>	$87.98 \pm 2.33$	$89.36 \pm 1.78$	$86.33 \pm 2.95$	<b><math>91.66 \pm 1.52</math></b>
$t_1 \rightarrow t_3$	$76.44 \pm 2.66$	$80.48 \pm 2.73$	<b><math>94.97 \pm 1.29</math></b>	$84.20 \pm 4.29$	$94.80 \pm 0.87$	$83.91 \pm 3.24$	<b><math>93.17 \pm 1.89</math></b>
$t_2 \rightarrow t_3$	$67.12 \pm 1.28$	$72.02 \pm 1.32$	$85.83 \pm 1.31$	$80.58 \pm 2.10$	<b><math>87.92 \pm 1.87</math></b>	$82.65 \pm 1.87$	<b><math>89.01 \pm 2.38</math></b>
hallway1	$60.02 \pm 2.60$	$65.93 \pm 0.86$	$76.36 \pm 2.44$	$77.48 \pm 2.68$	<b><math>86.98 \pm 2.02</math></b>	<b><math>85.50 \pm 2.92</math></b>	-
hallway2	$49.38 \pm 2.30$	$62.44 \pm 1.25$	$64.69 \pm 0.77$	<b><math>78.54 \pm 1.66</math></b>	<b><math>87.74 \pm 1.89</math></b>	$76.14 \pm 2.45$	-
hallway3	$48.42 \pm 1.32$	$59.18 \pm 0.56$	$65.73 \pm 1.57$	$75.10 \pm 3.39$	<b><math>82.02 \pm 2.34</math></b>	<b><math>76.04 \pm 2.55</math></b>	-

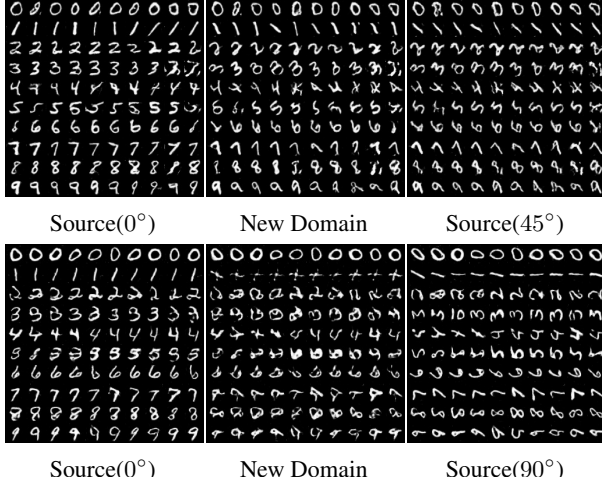


Figure 4. Generated images from our model. The first row shows the generated images in source domains  $D_{0^\circ}$  and  $D_{45^\circ}$  and the new domain. The second row shows the generated images in source domains  $D_{0^\circ}$  and  $D_{90^\circ}$  and the new domain. An animated illustration is provided in Supplementary Material.

a straight-line hallway area.

For both tasks, we implement our GDAN by using a MLP with one hidden layer (128 nodes) for the generator  $g$  and set the dimension of input noise  $E$  and  $\theta$  to 20 and 1, respectively. In the first task, since the causal structure is stable across domains, we also apply the proposed C-GDAN constructed according to the learned causal structure from the source domains. Sec. 3 in Supplementary Material shows a causal graph obtained by the CD-NOD method on  $t_1$  and  $t_2$  datasets. We use a MLP with one hidden layer (64 nodes) to model  $g$  for each causal module. The dimensions of  $E$  and  $\theta$  are set to 1 for all the modules.

We also compare our methods with KMM, surrogate kernels (SuK) (Zhang Kai et al., 2013), TCA (Pan et al., 2011), DIP (Baktashmotlagh et al., 2013), and CTC (Gong et al., 2016). We follow the evaluation procedures described in (Zhang Kai et al., 2013). The performances of different methods are shown in Table 1. It can be seen that our method C-GDAN outperforms existing methods in the first task, demonstrating the benefits of incorporating causal structures in generative

Table 2. Comparison of different methods on MNIST-USPS.

CORAL	DAN	DANN	DSN	CoGAN	GDAN
81.7	81.1	91.3	91.2	95.7	<b>95.9</b>

modeling for domain transfer.

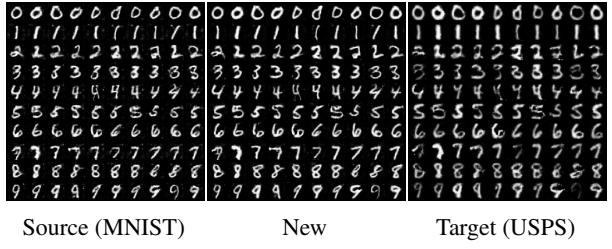


Figure 5. Generated images on the source, new, and target domain. An animated illustration is provided in Supplementary Material.

### 6.3. MNIST-USPS

USPS is another handwritten digit dataset including ten classes 0 – 9 with 7,291 training images and 2,007 test images. The original image resolution is  $16 \times 16$ . Following (Liu & Tuzel, 2016), we first increase the image size to  $20 \times 20$  by padding and then rescale the images to  $28 \times 28$ . In order to use the DCGAN structure, we further rescale both MNIST and USPS images to  $32 \times 32$ . Even after rescaling, there still exists a slight scale change between domains. We use the standard training-test splits for both MNIST and USPS. We compare our method with CORAL (Sun & Saenko, 2016), DAN (Long et al., 2015), DANN (Ganin et al., 2016), DSN (Bousmalis et al., 2016), and CoGAN (Liu & Tuzel, 2016). We adopt the discriminator in CoGAN for classification by training on the generated labeled images from our GDAN model. The quantitative results are shown in Table 2. It can be seen that our method achieves similar performance to CoGAN and outperforms the other methods. It should be noted that we use the standard DCGAN architecture while CoGAN uses a more complicated structure designed for this task.

In addition, we provide qualitative results to demonstrate our model’s ability to generate new domains. As shown in

Figure 5, we generate a new domain in the middle of MNIST and USPS. The images on the new domain have slightly larger scale than those on MNIST and slightly smaller scale than those on USPS, indicating that our model understands how the domain changes. Although the slight scale change is not easily distinguishable by human eyes, it can cause a performance degradation in terms of classification accuracy.

## 7. Conclusion

We have shown how deep learning and causal graph meet, play their roles in the same framework, and address the challenging domain adaptation problem. First, we proposed a generative domain adaptation network which is able to understand distribution changes and generate new domains. The proposed generative model also demonstrates promising performance in single-source domain adaptation. Second, by incorporating reasonable causal structure into the model and making use of modularity, we obtain a clear reduction of model complexity and improve the transfer efficiency.

## References

Baktashmotagh, M., Harandi, M.T., Lovell, B.C., and Salzmann, M. Unsupervised domain adaptation by domain invariant projection. In *Computer Vision (ICCV), 2013 IEEE International Conference on*, pp. 769–776, Dec 2013. doi: 10.1109/ICCV.2013.100.

Bousmalis, Konstantinos, Trigeorgis, George, Silberman, Nathan, Krishnan, Dilip, and Erhan, Dumitru. Domain separation networks. In *Advances in Neural Information Processing Systems*, pp. 343–351, 2016.

Bousmalis, Konstantinos, Silberman, Nathan, Dohan, David, Erhan, Dumitru, and Krishnan, Dilip. Unsupervised pixel-level domain adaptation with generative adversarial networks. In *Proceedings of the IEEE Conference on Computer Vision and Pattern Recognition*, pp. 3722–3731, 2017.

Cortes, C., Mansour, Y., and Mohri, M. Learning bounds for importance weighting. In *NIPS 23*, 2010.

Courty, Nicolas, Flamary, Rémi, Habrard, Amaury, and Rakotomamonjy, Alain. Joint distribution optimal transportation for domain adaptation. In *Advances in Neural Information Processing Systems*, pp. 3733–3742, 2017a.

Courty, Nicolas, Flamary, Rémi, Tuia, Devis, and Rakotomamonjy, Alain. Optimal transport for domain adaptation. *IEEE transactions on pattern analysis and machine intelligence*, 39(9):1853–1865, 2017b.

Ganin, Yaroslav, Ustinova, Evgeniya, Ajakan, Hana, Germain, Pascal, Larochelle, Hugo, Laviolette, François, Marchand, Mario, and Lempitsky, Victor. Domain-adversarial training of neural networks. *The Journal of Machine Learning Research*, 17(1):2096–2030, 2016.

Gong, M., Zhang, K., Liu, T., Tao, D., Glymour, C., and Schölkopf, B. Domain adaptation with conditional transferable components. In *Proceedings of the 33rd International Conference on Machine Learning (ICML 2016)*, volume 48, pp. 2839–2848, 2016.

Goodfellow, Ian, Pouget-Abadie, Jean, Mirza, Mehdi, Xu, Bing, Warde-Farley, David, Ozair, Sherjil, Courville, Aaron, and Bengio, Yoshua. Generative adversarial nets. In *Advances in neural information processing systems*, pp. 2672–2680, 2014.

Huang, J., Smola, A., Gretton, A., Borgwardt, K., and Schölkopf, B. Correcting sample selection bias by unlabeled data. In *NIPS 19*, pp. 601–608, 2007.

Iyer, A., Nath, A., and Sarawagi, S. Maximum mean discrepancy for class ratio estimation: Convergence bounds and kernel selection. In *Proc. ICML 2014*, 2014.

Kim, Taeksoo, Cha, Moonsu, Kim, Hyunsoo, Lee, Jungkwon, and Kim, Jiwon. Learning to discover cross-domain relations with generative adversarial networks. *arXiv preprint arXiv:1703.05192*, 2017.

Li, Chun-Liang, Chang, Wei-Cheng, Cheng, Yu, Yang, Yiming, and Póczos, Barnabás. Mmd gan: Towards deeper understanding of moment matching network. *arXiv preprint arXiv:1705.08584*, 2017a.

Li, Chunyuan, Liu, Hao, Chen, Changyou, Pu, Yunchen, Chen, Liqun, Henao, Ricardo, and Carin, Lawrence. Alice: Towards understanding adversarial learning for joint distribution matching. *Neural Information Processing Systems (NIPS)*, 2017b.

Li, Yujia, Swersky, Kevin, and Zemel, Rich. Generative moment matching networks. In *International Conference on Machine Learning*, pp. 1718–1727, 2015.

Liu, Ming-Yu and Tuzel, Oncel. Coupled generative adversarial networks. In *Advances in neural information processing systems*, pp. 469–477, 2016.

Liu, Ming-Yu, Breuel, Thomas, and Kautz, Jan. Unsupervised image-to-image translation networks. In *Advances in Neural Information Processing Systems*, pp. 700–708, 2017.

Long, M., Cao, Y., Wang, J., and Jordan, M. Learning transferable features with deep adaptation networks. In Blei, David and Bach, Francis (eds.), *Proceedings of the 32nd International Conference on Machine Learning (ICML-15)*, pp. 97–105. JMLR Workshop and Conference Proceedings, 2015. URL <http://jmlr.org/proceedings/papers/v37/long15.pdf>.

Long, Mingsheng, Zhu, Han, Wang, Jianmin, and Jordan, Michael I. Deep transfer learning with joint adaptation networks. In *International Conference on Machine Learning*, pp. 2208–2217, 2017.

Muandet, Krikamol, Fukumizu, Kenji, Sriperumbudur, Bharath, Schölkopf, Bernhard, et al. Kernel mean embedding of distributions: A review and beyond. *Foundations*

and Trends® in Machine Learning, 10(1-2):1–141, 2017.

Pan, S. J., Tsang, I. W., Kwok, J. T., and Yang, Q. Domain adaptation via transfer component analysis. *IEEE Transactions on Neural Networks*, 22:199–120, 2011.

Pearl, J. *Causality: Models, Reasoning, and Inference*. Cambridge University Press, Cambridge, 2000.

Radford, Alec, Metz, Luke, and Chintala, Soumith. Unsupervised representation learning with deep convolutional generative adversarial networks. *arXiv preprint arXiv:1511.06434*, 2015.

Shimodaira, H. Improving predictive inference under covariate shift by weighting the log-likelihood function. *Journal of Statistical Planning and Inference*, 90:227–244, 2000.

Song, L., Fukumizu, K., and Gretton, A. Kernel embeddings of conditional distributions. *IEEE Signal Processing Magazine*, 30:98 – 111, 2013.

Spirites, P., Glymour, C., and Scheines, R. *Causation, Prediction, and Search*. MIT Press, Cambridge, MA, 2nd edition, 2001.

Storkey, A. When training and test sets are different: Characterizing learning transfer. In Candela, J., Sugiyama, M., Schwaighofer, A., and Lawrence, N. (eds.), *Dataset Shift in Machine Learning*, pp. 3–28. MIT Press, 2009.

Sugiyama, M., Suzuki, T., Nakajima, S., Kashima, H., von Bünau, P., and Kawanabe, M. Direct importance estimation for covariate shift adaptation. *Annals of the Institute of Statistical Mathematics*, 60:699–746, 2008.

Sun, Baochen and Saenko, Kate. Deep coral: Correlation alignment for deep domain adaptation. In *European Conference on Computer Vision*, pp. 443–450. Springer, 2016.

Tieleman, Tijmen and Hinton, Geoffrey. Lecture 6.5-rmsprop: Divide the gradient by a running average of its recent magnitude. *COURSERA: Neural networks for machine learning*, 4(2):26–31, 2012.

Tzeng, Eric, Hoffman, Judy, Zhang, Ning, Saenko, Kate, and Darrell, Trevor. Deep domain confusion: Maximizing for domain invariance. *arXiv preprint arXiv:1412.3474*, 2014.

Yu, Y. and Szepesvári, C. Analysis of kernel mean matching under covariate shift. In *Proceedings of the 29th International Conference on Machine Learning (ICML-12)*, pp. 607–614, 2012.

Zhang, K., Peters, J., Janzing, D., and Schölkopf, B. Kernel-based conditional independence test and application in causal discovery. In *Proceedings of the 27th Conference on Uncertainty in Artificial Intelligence (UAI 2011)*, Barcelona, Spain, 2011.

Zhang, K., Schölkopf, B., Muandet, K., and Wang, Z. Domain adaptation under target and conditional shift. In *Proceedings of the 30th International Conference on Machine Learning, JMLR: W&CP Vol. 28*, 2013.

Zhang, Kun, Huang, Biwei, Zhang, Jiji, Glymour, Clark, and Schölkopf, Bernhard. Causal discovery from non-stationary/heterogeneous data: Skeleton estimation and orientation determination. In *IJCAI: proceedings of the conference*, volume 2017, pp. 1347. NIH Public Access, 2017.

Zhang Kai, Zhang., Zheng, V., Wang, Q., Kwok, J., Yang, Q., and Marsic, I. Covariate shift in hilbert space: A solution via surrogate kernels. In *Proceedings of the 30th International Conference on Machine Learning*, pp. 388–395, 2013.

Zhu, Jun-Yan, Park, Taesung, Isola, Phillip, and Efros, Alexei A. Unpaired image-to-image translation using cycle-consistent adversarial networks. *arXiv preprint arXiv:1703.10593*, 2017.

# Supplement to “Causal Generative Domain Adaptation Networks”

This supplementary material provides the proofs and some details which are omitted in the submitted paper. The equation numbers in this material are consistent with those in the paper.

## S1. Proof of Theorem 1

*Proof.* Since  $P_Y$  does not change, if  $P_{XY}^s = Q_{XY}^s$  after distribution matching, we have  $P_{X|Y=y}^s = Q_{X|Y=y}^s, \forall y \in \mathcal{Y}$ . For a given  $y$ , the label-conditional distribution on the  $s$ -th domain is  $P_{X|Y=y}^s = \mathcal{N}(A_2y + A_3\theta_s, A_1A_1^\top)$ . Similarly, label-conditional distribution of the model is  $P_{X|Y=y}^s = \mathcal{N}(\hat{A}_2y + \hat{A}_3\hat{\theta}_s, \hat{A}_1\hat{A}_1^\top)$ . By moment matching, we have

$$A_2y + A_3\theta_s = \hat{A}_2y + \hat{A}_3\hat{\theta}_s, \quad (15)$$

$$A_1A_1^\top = \hat{A}_1\hat{A}_1^\top. \quad (16)$$

It can be seen from (16) that  $\hat{A}_1 = A_1R$ , where  $R$  is a rotation matrix. Let  $z_s = A_3\theta_s$ , we consider the noiseless factor analysis (FA) model with bias:  $Z = \hat{A}_3\hat{\theta} + (\hat{A}_2 - A_2)y$ . Then, given  $m$  source domains, we have  $m$  examples  $\{(z_s, \hat{\theta}_s)\}_{s=1}^m$  drawn from the FA model. According to A4, we have  $\hat{A}_2 = A_2 + \frac{1}{my} \sum_{s=1}^m z_s$ . Thus, as  $m \rightarrow \infty$ ,  $\hat{A}_2 = A_2$ . Let  $\bar{z}_s = z_s - \frac{1}{m} \sum_{s=1}^m z_s$ , because  $\text{rank}(\Theta) \geq d+1$ , we can find the  $d$  eigenvectors  $\{u_i\}_{i=1}^d \in \mathbb{R}^D$  of  $\hat{C}_Z = \frac{1}{m-1} \sum_{s=1}^m \bar{z}_s \bar{z}_s^\top$  corresponding to its  $d$  non-zero eigenvalues. Then,  $\hat{A}_3 = U_z R$ , where  $U_z = [u_1, \dots, u_d] \in \mathbb{R}^{D \times d}$  and  $R$  is a rotation matrix. Therefore, we have

$$\forall s, \hat{\theta}_s = \hat{A}_3^\top A_3\theta_s - \hat{A}_3^\top (\hat{A}_2 - A_2)y, \quad (17)$$

Because both  $A_3$  and  $\hat{A}_3$  are full column rank,  $\hat{A}_3^\top A_3$  is invertible. Thus we can obtain  $\theta_s = (\hat{A}_3^\top A_3)^{-1}\hat{\theta}_s + (\hat{A}_3^\top A_3)^{-1}\hat{A}_3^\top (\hat{A}_2 - A_2)y, \forall s$ , meaning that  $\hat{\theta}$  is a one-to-one mapping of  $\theta$ .  $\square$

## S2. Proof of Theorem 2

*Proof.* According to the sum rule, we have

$$\begin{aligned} P_{X|\theta} &= \sum_{c=1}^C P_{X|Y=c, \theta} P_{Y=c}, \\ P_{X|\theta'} &= \sum_{c=1}^C P_{X|Y=c, \theta'} P'_{Y=c}. \end{aligned} \quad (18)$$

Since  $P_{X|\theta} = P_{X|\theta'}$ , then

$$\sum_{c=1}^C P_{X|Y=c, \theta} P_{Y=c} = \sum_{c=1}^C P_{X|Y=c, \theta'} P'_{Y=c}.$$

Also, because A5 holds true, we have

$$P_{X|Y=c, \theta} P_{Y=c} - P_{X|Y=c, \theta'} P'_{Y=c} = 0. \quad (19)$$

Taking the integral of (19) leads to  $P_Y = P'_Y$ , which further implies that  $P_{X|Y, \theta} = P_{X|Y, \theta'}$ .  $\square$

## S3. Causal Structure on WiFi Data

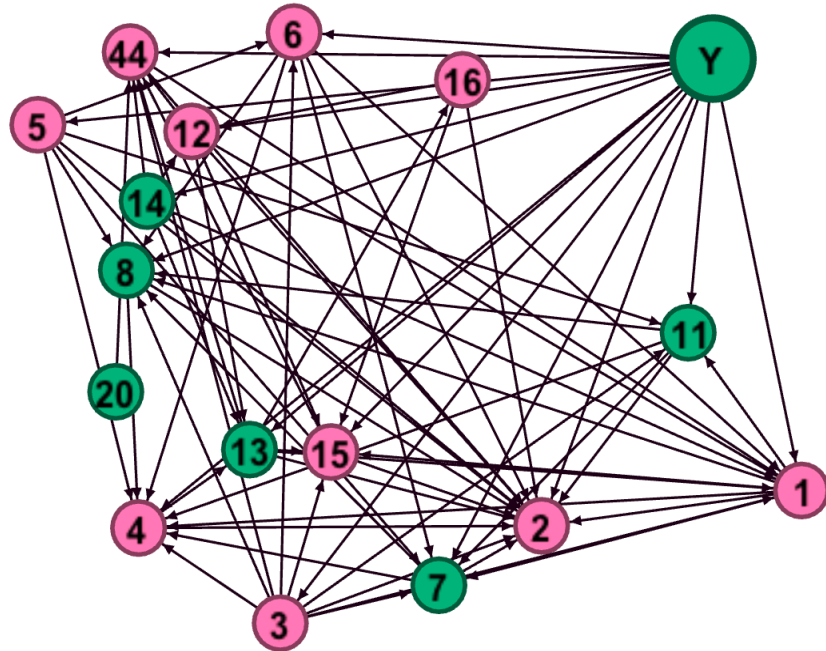


Figure 6. The causal structure learned by CD-NOD on the WiFi t1 and t2 datasets. Pink nodes denote the changing modules and green ones denote the constant modules whose conditional distribution does not change across domains.